Sievert, L, Stancioiu, D and Matthews, C

Active Vibration Control of a Small-Scale Flexible Structure Subject to Moving-Loads and Experimental Validation

Authors: Sievert, Lukas, Stancioiu, Dan and Matthews, Christian

ASME Journal Title: Journal of Vibration and Acoustics

Volume/Issue __143(6)___________________________ Date of Publication (VOR* Online) ___4/5/2021_______________

ASME Digital Collection URL: https://asmedigitalcollection.asme.org/vibrationacoustics/article-abstract/143/6/061010/1107009/Active-Vibration-Control-of-a-Small-Scale-Flexible?redirectedFrom=fulltext

DOI: https://doi.org/10.1115/1.4050852

*VOR (version of record)

Author Manuscript

Published in final edited form as:

J. Vib. Acoust. , **143**(6), 2021, DOI: 10.1115/1.4050852

Active vibration control of a small-scale flexible structure subject to moving-loads and experimental validation

Lukas Sievert

Department of Maritime and Mechanical Engineering, Liverpool John Moores University,3 Byrom Street, L3 3AF, Liverpool, United Kingdom
e-mail: l.sievert@2017.ljmu.ac.uk

Dan Stancioiu

Department of Maritime and Mechanical Engineering, Liverpool John Moores University,3 Byrom Street, L3 3AF, Liverpool, United Kingdom
e-mail: d.stancioiu@ljmu.ac.uk

Christian Matthews

Department of Maritime and Mechanical Engineering, Liverpool John Moores University,3 Byrom Street, L3 3AF, Liverpool, United Kingdom
Email: c.matthews@ljmu.ac.uk

Abstract

This study directly addresses the problem of optimal control of a structure under the action of moving masses. The main objective is to experimentally implement and validate an active control solution for a small-scale test stand. The supporting structure is modeled as an Euler-Bernoulli simply supported beam, acted upon by moving masses of different weights and velocities. The experimental implementation of the active controller posces a particular set of challenges as compared to the numerical solutions.

It is shown both numerically and experimentally that using electromagnetic actuation, a reduced order controller designed using a time-varying algorithm provides a reduction of the maximum deflection of up to 18% as compared to the uncontrolled structure. The controller performance and robustness were tested against a representative set of possible moving load parameters.

In consequence of the variations in moving mass weight and speed the controller gain requires a supplementary adaptation. A simple algorithm that schedules the gain as a function of the weight and speed of the moving mass can achieve both a good performance and an adjustment of the control effort to the specific design requirements.

Keywords:

Time-varying optimal control, Active vibration control, Moving mass, State estimation

1. Introduction

The dynamics of a structure under the action of a moving load is relevant to many engineering applications such as linear guideways, robotics and overhead cranes. However, this subject is particularly studied and applied to vehicle/pedestrian-bridge interaction and train-track interaction [1–5]. If the inertia effect of the moving structure needs to be taken into account [6], in modal space it leads to a time-varying system of equations. The problem of moving loads in relation to bridge-structure interaction has been studied extensively both analytically and experimentally [7,8]. Of special concern for structural engineers is not only the modelling but also for the improvement of the dynamic response of the supporting structure to specific moving-load actions. One example could be the effect of different traffic loads in the case of a bridge structure. The research literature shows a series of studies that put forward passive methods designed to address this specific problem. The passive approach is attractive as it provides a low cost solution [9–12], but it is less efficient when the structure is subjected to loads with a random variation in parameters like moving speed and weight.

Active vibration control methods offer higher efficiency by reducing broadband frequencies and by providing a higher and flexible actuation [13] which in the context of a moving mass structure means that the control could adapt actively to different weights and speeds. The active control of a structure subjected to a moving mass, compared to the general structural modal control [14–16], is of special interest and difficulty. The dynamic matrices of the structure, mass, damping and stiffness change over time, depending on the speed and weight of the moving mass, therefore an active control solution must take into account the time-varying nature of the system [17–19].

Several studies have investigated the active control of a moving mass system numerically. Sung [20] presented the dynamic modelling and the time-invariant optimal control of a simply supported beam under a moving mass. He used two piezoelectric actuators and their locations were determined by an optimal quadratic cost functional. Deng et al. [21] used a linear-quadratic Gaussian modal controller for a time-varying structure including identification and control update in real-time. The numerical model, which alters due to structural changes, is updated by an observer. The method was validated numerically.

The time-varying nature of the system was taken into account in [18] where Nikkhoo proposes a method based on solving the Riccati equation at every time-step. In [17,18] it is shown that for a high traveling speed, and for certain locations and number of actuators, the time-varying control shows a significant improvement compared to the time-invariant control. In [19] the classical optimal control approach is applied to single and multi-span beams under the influence of a moving load and a moving mass. The proposed solutions were based on displacement-velocity and velocity-acceleration feedback using piezoelectric actuators. Stancioiu et al. [17] cast the problem into a terminal-time optimal control framework [22] and further presented a numerical study for synthesis of time-varying control solution. The study also introduced an augmented system, which took into account the effect of the moving mass in the control synthesis problem. A drawback of the study was that it assumed full knowledge of the state-variables. A combination of sliding mode control and positive position feedback for a beam subjected to a moving mass was presented in [23]. The sliding mode control, used when the mass moves along the beam is robust to parameter uncertainties and the positive position feedback control is efficient to suppress the free vibration after the mass leaves the beam. Liu et. al. [24] devised a finite-time optimal regulator for an uncertain beam-mass system. The distributed material parameters were discretized for representative points and the regulator calculated with the probability density equation method.

Despite a large number of studies dedicated to numerical solutions, only few studies approached the problem of experimental implementation and validation of the moving mass vibration control. One of the main difficulties for the experimental implementation of the controller is that if the dynamic equations are cast in modal space, the states are not directly accessible. Therefore an observer or state-estimator needs to be considered. This in turn leads to high computational time which counteracts the real-time ability of the controller. Frischgesell et. al. [25] studied a time-varying discrete observer for a moving mass system equipped with a force actuator. The aim was to minimize the maximum traverse deflection. The time-varying system and input matrices were calculated offline at specific times due to the high computation time required. Reckkmann and Popp [26] extend this work with an adaptation method and a discrete time optimal controller designed to achieve a lower deflection of the flexible structure.

Pisarski [27] studied numerically and experimentally the semi-active control of a structure subjected to a moving load. In this study, an open-loop optimal bang-bang controller was used. The study considered the moving speed and weight of the mass and it was shown that the controlled system outperforms the passive case by 40% in terms of the proposed evaluation metric. This work was extended by [28] where a closed-loop adaptive control was proposed. The control gains were calculated offline for a constant speed and mass of the load with the ability to adapt online to the actual mass parameters.

This paper presents an experimental approach to the problem of active control of a structure under moving loads. The proposed solution is based on an optimal time-varying control algorithm and relies on a state-feedback controller. A new method to estimate the states of the system (modal coordinates and modal velocities) based on the inverse of the matrix of modal shape vectors and measured displacements is proposed. This simpler algorithm allows fast sampling times and proves to be robust against structural changes. This method of state estimation was first presented by the authors in [29], where a suboptimal controller was implemented to reduce the deflection of the beam at given locations.

In spite of the fact that the time-varying nature of the system is taken into account in the control approach, an objective function based on deflection responses requires an adaptation of the control effort to the mass and velocities of the load acting on the supporting structure. The feasibility of a simple gain scheduling procedure is investigated and shows a good performance for a control effort adjusted to the dynamic parameters of the problem.

2. The moving-mass structure interaction model

The investigated structure is modelled as an Euler-Bernoulli simply supported beam structure of mass per unit length ρA and flexural rigidity EI. The structure of length L is subjected to the action of a mass m moving with constant speed v, as illustrated in Fig. 1. The structure is also supported by an inertial shaker which in passive state will be modelled as a spring-damper support. In the active state the actuator dynamics is represented by a transfer function *H(s)*, specified in state space form in Eq. (5).

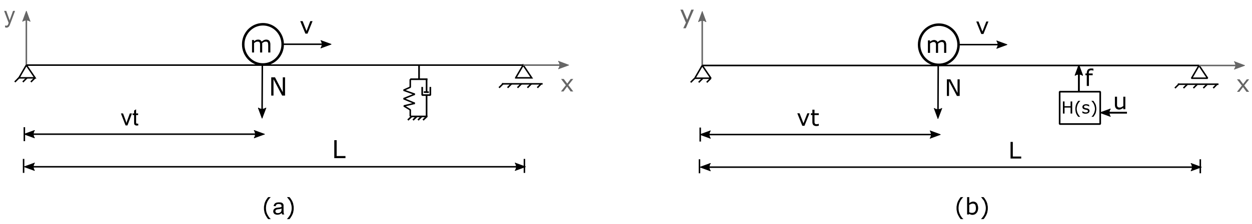

Fig. 1 Model of the beam structure subjected to a moving mass, with an inactive actuator (a) and an active actuator (b).

Under the assumption of permanent contact between the mass and the beam, the general system of equations in modal coordinates governing the dynamics of a beam subjected to a mass *m* travelling at constant speed *v* at any time *t* within the interval $[0,t_f]$ with $t_f = L/v$ is [2,29,30]:

$$(\mathbf{M}+\Delta\mathbf{M}(t))\ddot{\mathbf{q}}+(\mathbf{D}+\Delta\mathbf{D}(t)+\mathbf{D_a})\dot{\mathbf{q}}+(\mathbf{K}+\Delta\mathbf{K}(t)+\mathbf{K_a})\mathbf{q}=-mg\boldsymbol{\psi}(vt)+\boldsymbol{\psi}(x_a)f \tag{1}$$

In this case the vectors $\mathbf{q}$ and $\dot{\mathbf{q}}$ represent modal displacements and modal velocities of the structure which are not directly accessible from the measurements and are estimated using mode shape functions. The structure's response is approximated at sensor locations x_{si} using the mode shape functions $\boldsymbol{\psi}(x)$, as: $w(x_{si},t)=\boldsymbol{\psi}^{\mathrm{T}}(x_{si})\mathbf{q}(t)$. The constant matrices $\mathbf{M}$, $\mathbf{D}$ and $\mathbf{K}$ can be expressed as functions of the modal shape vectors $\boldsymbol{\psi}(x)$, mass per unit length ρA, damping $c\rho A$ and stiffness EI:

$$\mathbf{M} = \rho A \int_0^{\mathrm{L}} \boldsymbol{\psi}(x)\, \boldsymbol{\psi}^{\mathrm{T}}(x)\mathrm{d}x\,,$$

$$\mathbf{D} = \rho A c \int_0^{\mathrm{L}} \boldsymbol{\psi}(x)\, \boldsymbol{\psi}'^{\mathrm{T}}(x)\mathrm{d}x\,, \tag{2}$$

$$\mathbf{K} = EI \int_0^{\mathrm{L}} \boldsymbol{\psi}(x)\, \boldsymbol{\psi}''''^{\,\mathrm{T}}(x)\mathrm{d}x$$

The time-dependent matrices $\Delta\mathbf{M}(t)$, $\Delta\mathbf{D}(t)$ and $\Delta\mathbf{K}(t)$ are defined as [17,30]:

$$\Delta\mathbf{M}(t) = m\, \boldsymbol{\psi}(vt)\, \boldsymbol{\psi}^{\mathrm{T}}(vt)\,,$$

$$\Delta\mathbf{D}(t) = 2mv\, \boldsymbol{\psi}(vt)\, \boldsymbol{\psi}'^{\mathrm{T}}(vt)\,, \tag{3}$$

$$\Delta\mathbf{K}(t) = mv^2\, \boldsymbol{\psi}(vt)\, \boldsymbol{\psi}''^{\mathrm{T}}(vt)$$

The added damping and stiffness matrices due to the electrodynamic actuator located at x_a are [29]:

$$\mathbf{D_a} = c_a \boldsymbol{\psi}\,(\boldsymbol{x_a})\boldsymbol{\psi}^{\mathrm{T}}(x_a)\,,$$

$$\mathbf{K_a} = k_a \boldsymbol{\psi}(\boldsymbol{x_a})\boldsymbol{\psi}^{\mathrm{T}}(x_a) \tag{4}$$

An accurate model of the modal shaker could be very complex [27]. For this investigation a simpler first order model valid at low frequencies is used. The dynamics of the actuator acting on the beam structure is modelled as a state-space system from input voltage u to output force f:

$$\dot{z} = -\alpha z + \beta u;$$

$$f = \gamma z \tag{5}$$

In the state-space representation, considering n vibrational modes, with inclusion of the electrodynamic shaker's dynamics, the system matrices are:

$$\mathbf{A}(t) = \begin{bmatrix} \mathbf{0}_{n\times n} & \mathbf{I}_{n\times n} & \mathbf{0}_{nx1} \\ -(\mathbf{M}+\Delta\mathbf{M}(t))^{-1}(\mathbf{K}+\Delta\mathbf{K}(t)+\mathbf{K_a}) & -(\mathbf{M}+\Delta\mathbf{M}(t))^{-1}(\mathbf{D}+\Delta\mathbf{D}(t)+\mathbf{D_a}) & \gamma(\mathbf{M}+\Delta\mathbf{M}(t))^{-1}\boldsymbol{\psi}(x_a)] \\ \mathbf{0}_{1\times n} & \mathbf{0}_{1\times n} & -\alpha \end{bmatrix}; \tag{6}$$

$$\mathbf{B} = \begin{bmatrix} \mathbf{0}_{n\times 1} \\ \mathbf{0}_{n\times 1} \\ \beta \end{bmatrix}; \;\; \mathbf{B_f}(t) = \begin{bmatrix} \mathbf{0}_{n\times 1} \\ -(\mathbf{M}+\Delta\mathbf{M}(t))^{-1}\boldsymbol{\psi}(vt) \\ 0 \end{bmatrix};$$

The state vector becomes $\mathbf{x}^{\mathbf{T}}(t)=[\mathbf{q}(t)\ \dot{\mathbf{q}}(t)\ z(t)]$. The time t_f represents the time the mass leaves the beam. From this instant of time, the beam vibrates freely and the system governing the motion is a linear-time invariant system. The system equations for $t > t_f$ changes from (1) to:

$$\mathbf{M}\ddot{\mathbf{q}}+\mathbf{D}\dot{\mathbf{q}}+\mathbf{K}\mathbf{q}= \boldsymbol{\psi}(x_a)f \tag{7}$$

with initial conditions the values of the states at the instant of time t_f.

3. The finite time control algorithm

When only one actuator is used, the time-varying plant with the states and control matrices presented in (6), can be written in state-space form as:

$$\dot{\mathbf{x}}(t) = \mathbf{A}(t)\mathbf{x}(t) + \mathbf{B}(t)u(t) \tag{8}$$

The aim of the controller is to minimize the deflection response at different locations along the beam. In order to achieve this the performance objective can be formulated like a quadratic objective in deflection at sensors locations

$$J = \frac{1}{2}\int_{t_0}^{t_f} \mathbf{w}^{\mathrm{T}}(x_{si},t)\mathbf{Q}\,\mathbf{w}(x_{si},t)dt = \frac{1}{2}\int_{t_0}^{t_f} \mathbf{x}^{\mathrm{T}}(t)\mathbf{C}^{\mathrm{T}}\mathbf{Q}\,\mathbf{C}\,\mathbf{x}(t)dt \tag{9}$$

subject to equation (8) and the control's saturation limits $|u(t)| \leq u_0$. In equation (9) matrix **C** is the output matrix of the system described by (8) and consists of modal shape vectors $\boldsymbol{\psi}(x_{si})$.

This type of objective function was studied in [17] and it was shown that it leads to a two-boundary value problem which makes the control design problem mathematically challenging. Also, the synthesized control function is discontinuous. Such a control solution, even if it correctly describes the required control action, may be difficult to implement as the electromagnetic type of actuation chosen here cannot accurately describe a control function with discontinuities. For this reason, a quadratic objective function that also includes the control has been chosen. The quadratic performance index is defined as:

$$J = \frac{1}{2}\mathbf{x}^{\mathrm{T}}(t_f)\mathbf{F}\,\mathbf{x}(t_f) + \frac{1}{2}\int_{t_0}^{t_f}[\mathbf{x}^{\mathrm{T}}(t)\mathbf{Q}\,\mathbf{x}(t) + u^{\mathrm{T}}(t)\,\mathrm{R}\,u(t)]dt \tag{10}$$

The emphasis on the deflection will be addressed by choosing a state weighting matrix **Q** with higher values corresponding to the first states corresponding to the displacements and a significantly lower value for the terms corresponding to the velocities. The control limitation is assured by the selection of the control weighting parameter R. In equation (10) t_f is specified and the final state $\mathbf{x}(t_f)$ is constrained by the weighting matrix **F** in order to reduce the free vibration of the structure when one mass leaves the beam [17]**.** For a system with p states and r actuators, the matrices **F** and **Q** are $p \times p$ symmetric, positive semidefinite matrices and matrix **R** is $r \times r$ positive definite. For the case when only one actuator is used, R becomes a scalar. When the value of the control function $u(t)$ is unconstrained, the optimal control $u^*(t)$ is defined as [22] :

$$u^*(t) = -\mathrm{R}^{-1}\mathbf{B}'(t)\mathbf{P}(t)\mathbf{x}^*(t) \; = -\mathbf{k}(t)\mathbf{x}^*(t) \tag{11}$$

$\mathbf{k}(t) = -\mathrm{R}^{-1}\mathbf{B}^{\mathbf{T}}(t)\mathbf{P}(t)$ is called the Kalman gain and $\mathbf{P}(t)$, is a $p \times p$ symmetric, positive definite matrix (for all $t \in [t_0, t_f]$), and is the solution of the matrix differential Ricatti equation

$$\dot{\mathbf{P}}(t) = \mathbf{P}(t)\mathbf{A}(t) - \mathbf{A}^{\mathrm{T}}(t)\mathbf{P}(t) - \mathbf{Q} + \mathbf{P}(t)\mathbf{B}(t)\mathrm{R}^{-1}\mathbf{B}^{\mathbf{T}}(t)\mathbf{P}(t) \tag{12}$$

The optimal state is the solution of

$$\dot{\mathbf{x}}^{*}(t) = [\mathbf{A}(t) \ - \mathbf{B}(t)\mathrm{R}^{-1}\mathbf{B}^{\mathbf{T}}(t)\mathbf{P}(t)]\mathbf{x}^{*}(t) \tag{13}$$

The matrix differential Eq. (12) can be solved backwards with $t_{start}=t_f$ and the initial condition $\mathbf{P}(t=t_f)=\mathbf{F}$. Then the optimal time-varying gain $\mathbf{k}$(t) is calculated forward using the values of $\mathbf{P}$(t). Although p optimal states $x^{*}(t)$ are calculated, in theory the structure consists of an infinite number states which can cause instability. The performance of the control system still needs to be tested for a representative set of values of the masses and traveling speeds.

4. The state estimation

The particular type of problem studied here where the effect of the loads on the structure cannot be used as an input, makes the use of an estimator difficult. The solution presented here assumes that the number of sensors equals the number of modes used for the numerical model.

The state vector is estimated from the experimentally measured deflection vector $\mathbf{w}(t)_{\mathrm{n\ x\ 1}} = [w_1(x_{s1},t) \dots w_n(x_{sn},t)]^{\mathrm{T}}$ and the velocity vector $\dot{\mathbf{w}}(\mathrm{t})_{\mathrm{n\ x\ 1}} = [\dot{w}_1(x_{s1},t) \dots \dot{w}_n(x_{sn},t)]^{\mathrm{T}}$ at locations x_{sn} :

$$\begin{aligned} \mathbf{q}(t) &= \mathbf{\Psi}(x_{sn})^{-1}\mathbf{w}(t) \\ \dot{\mathbf{q}}(t) &= \mathbf{\Psi}(x_{sn})^{-1}\dot{\mathbf{w}}(t) \end{aligned} \tag{14}$$

In this equation $\mathbf{\Psi}(x_{sn})$ is the $n \times n$ matrix that contains the mode shapes calculated at sensor locations x_{sn}:

$$\mathbf{\Psi}(x_{sn})_{n\times n} = \begin{bmatrix} \psi_1(x_{s1}) & \psi_2(x_{s1}) & \dots & \psi_n(x_{s1}) \\ \psi_1(x_{s2}) & \psi_2(x_{s2}) & \dots & \psi_n(x_{s2}) \\ \vdots & \vdots & \ddots & \vdots \\ \psi_1(x_{sn}) & \psi_2(x_{sn}) & \dots & \psi_n(x_{sn}) \end{bmatrix} \tag{15}$$

When n sensors are used and n modes are estimated, the state-space vector can be determined as a unique solution of equations. From Eq. (14) and Eq. (15) it can be seen that only the mode shapes of the structure and the measured deflections are needed to calculate the modal coordinates and modal velocities. The advantage of this method is that it avoids the implementation of an observer and can be applied to time-varying systems with fast sampling times.

5. Experimental validation

In order to validate the beam-mass system modelled by Eq. (6), the method of state estimation of Eq. (14) and the finite time controller, numerical simulations are compared with experimental measurements.

5.1 The experimental test stand

Fig. 2. shows the experimental set-up. Different steel balls with known mass m are accelerated by a ramp and move over the simply supported beam structure at nearly constant speed. The geometrical characteristics of the aluminium beam are: span length L = 0.6 m and cross section A = 0.06 m × 0.002 m. By adding polymer guiding rails, the flexural rigidity and the damping coefficient are increased. Three displacement sensors measure the deflection at x_{s1}= 0.15 m, x_{s2} = 0.25 m and x_{s3} = 0.35 m.

The optimal gains of the finite time-varying and time-invariant control are calculated numerically in MATLAB and stored on a CompactRIO embedded controller. With input from the laser displacement sensors (optoNCDT 1700 and optoNCDT 1610), the states are estimated in real time every 15 ms and the output voltage is calculated and sent to the power amplifier (Data Physics PA30E) for the actuation of the electrodynamic shaker (Data Physics V4).

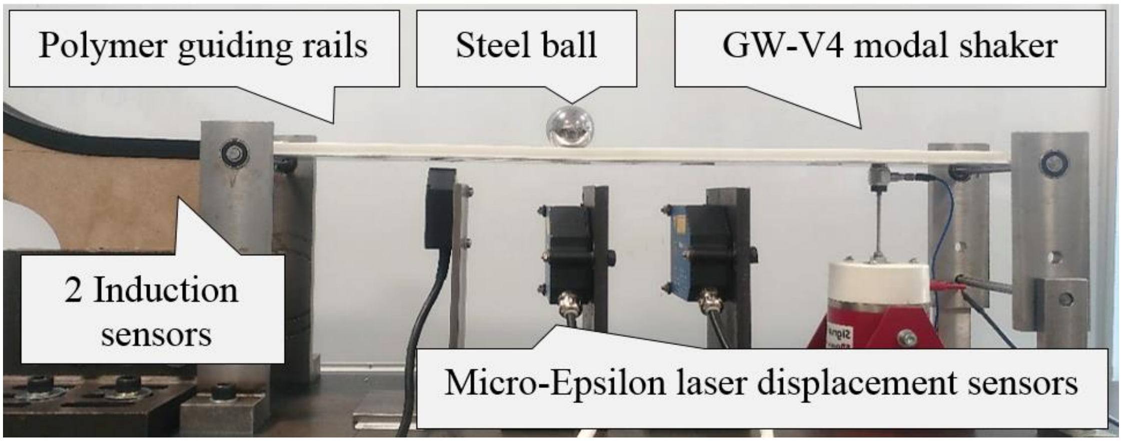

Fig. 2 Experimental set-up, aluminium polymer beam subjected to a moving mass.

Fig. 3 shows the deflection response $w(x_{si}, t)$, numerically estimated (blue line) at three sensor locations (i = 1, 2, 3) when 7 balls are launched along the beam, against the experimentally measured deflections (red line). For the last run two balls are moving on the structure. The parameters of the numerical beam model are defined as mass per length unit ρA = 0.535 kgm^{-1} and flexural rigidity $EI = 11.68\ \mathrm{Nm}^{-2}$. Due to the polymer guiding rail the height is changed to 3.3 mm and a constant modal damping ratio $\zeta = 0.03$ is assumed througout. No control action is involved. The influence of the electrodynamic actuator is modelled as a spring-damper system with a damping coefficient of c_a = 80 Nsm^{-1} and a stiffness of k_a = 12000 Nm^{-1}. With these adjustments, the deflections of the experimental data are in good agreement with the numerical model.

The beam-shaker system was validated using an active shaker with and without the action of the moving mass. Therefore, the shaker's stiffness changes to $k_\mathrm{a} = 3500\ \mathrm{Nm}^{-1}$ and $\gamma = 4.6$ in (5). Numerical investigations have shown that the dynamics of the beam can be accurately approximated using only the first three modes.

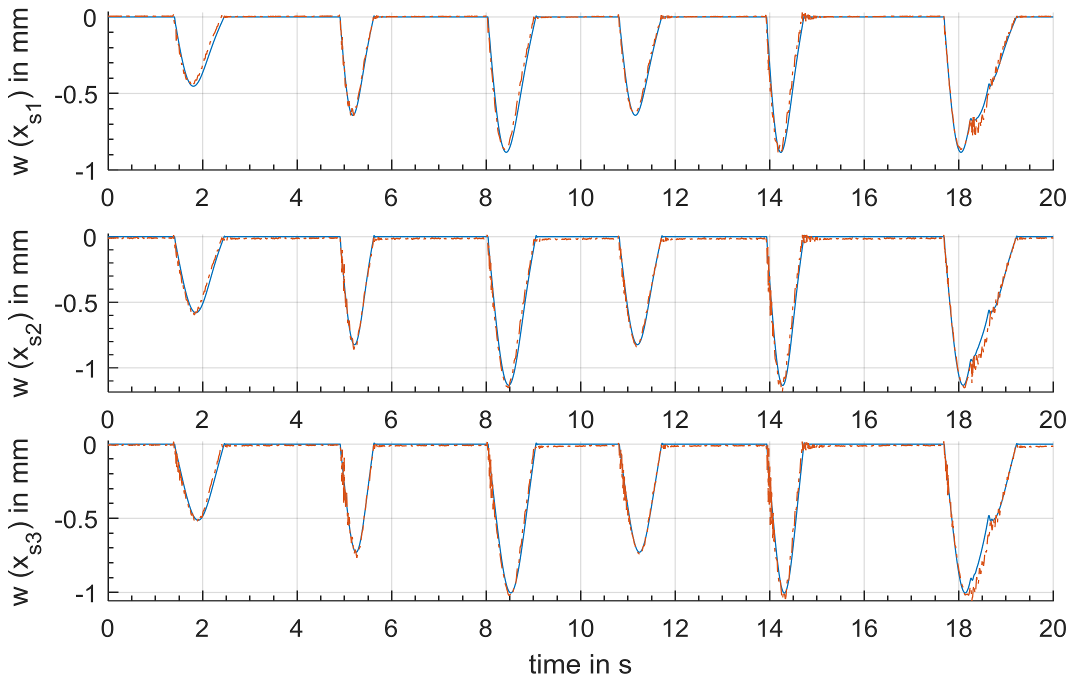

Fig. 3 Experimental validation between the displacements of masses traveling at different speeds obtained by the numerical model (blue continuous) and the experimental measurements (red dashed).

Fig. 4 shows a comparison between the experimental data and the numerical model for time deflection response at sensors locations when four masses are launched at different speeds along the beam and the shaker's input is fed with a prescribed voltage. In this case the voltage supplied was a combination of sinusoidal functions. From Eq. (14) and Eq. (15) it follows that, since three sensors are installed, three modal coordinates, q_i, ($i = 1,2,3$) can be calculated directly and by using the derivative three modal velocities, $\dot{q}_i$, ($i = 1,2,3$). For one mass moving along the beam these are represented in Fig. 5.

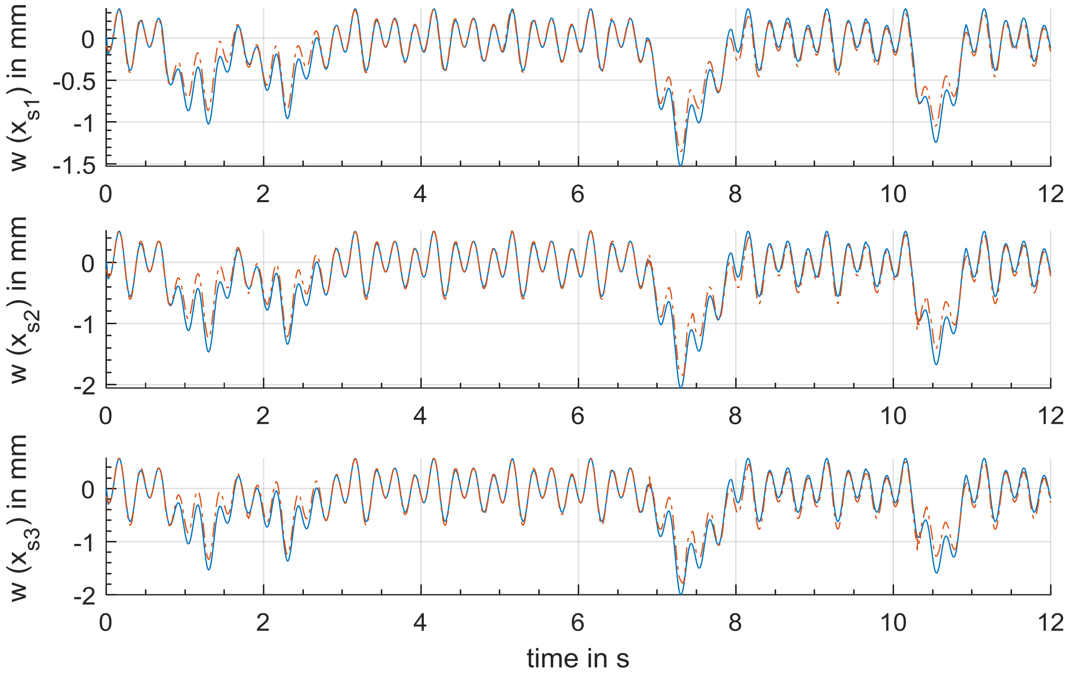

Fig. 4 Validation of the beam mass system with an active electromagnetic shaker, numerical model (blue continuous), and the experimental measurements (red dashed).

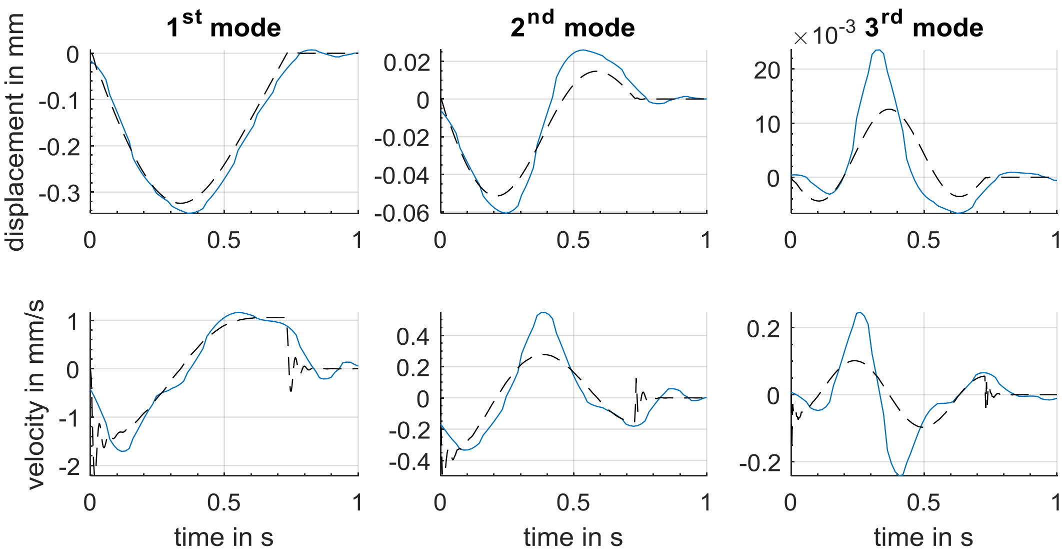

Fig. 5 Comparison modal coordinates and modal velocieties, numerical model (black dashed) and the measured signal (blue continuous).

The first mode is dominant and shows the best accordance with the modal displacement estimated using experimental data. For the modal velocity, the first mode also shows the best match. A 10th order digital low-pass filter with a cut-off frequency $f_{3dB} = 10$ Hz, reduces the noise but it causes a slight delay.

5.2 Experimental results for optimal control implementation

For the time-invariant control, the constant gain is calculated, without taking into account the time-varying parts in system equation (6):

$$\mathbf{A} = \begin{bmatrix} \mathbf{0}_{n\times n} & \mathbf{I}_{n\times n} & \mathbf{0}_{nxi} \\ -\mathbf{M}^{-1}\mathbf{K} & -\mathbf{M}^{-1}\mathbf{D} & \gamma\mathbf{M}^{-1}\boldsymbol{\psi}(x_a) \\ \mathbf{0}_{1\times n} & \mathbf{0}_{1\times n} & -\alpha \end{bmatrix}; \qquad \mathbf{B} = \begin{bmatrix} \mathbf{0}_{n\times 1} \\ \mathbf{0}_{n\times 1} \\ \beta \end{bmatrix}; \tag{16}$$

The actuator is located at x_a= 0.5 m. The error and performance index are defined as **Q**=diag(1000, 100, 10, 0.1, 0.01, 0.01, 0) and R = 0.00009 for the time-invariant control as well as for the time-varying control. The terminal cost matrix is defined as **F = Q**.

The displacement response of the supporting structure is mainly induced by the first mode. This knowledge was utilized by defining the error performance matrix **Q**, setting higher weight toward the first modes.

The weight of the moving masses used in the experiments ranges from 0.261 kg to 0.509 kg. The masses are accelerated by a ramp and move over the simply-supported beam structure with approximately constant speed. The values of the speeds used is between 0.3 ms^{-1} and 0.55 ms^{-1}.The actuator is located at x_a = 0.5 m, which is not the optimal position in terms of maximum deflection reduction making it even more necessary to employ the time-varying control solution [17]. The performance of the control methods is assessed by using the maximum absolute value of the displacement at the sensor locations x_{si}.

Of the three available sensor locations x_{s2} = 0.25 m is chosen for further evaluation of the control methods. It displays the maximum deflection of the beam, as seen in Fig. 3, as well as the maximum deflection at the moving coordinate *vt* (Fig. 6).

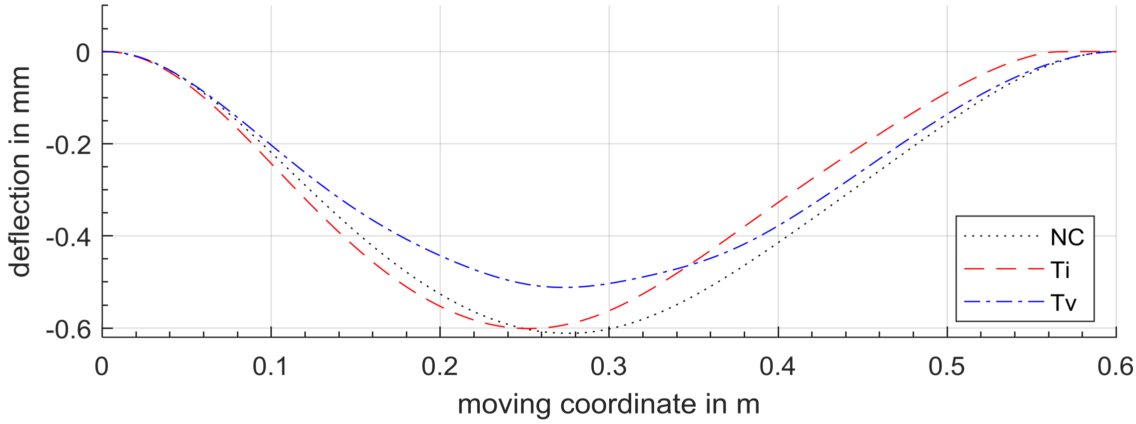

Fig. 6 Numerical deflection of the moving coordinate vt of the mass m = 0.5 kg traveling with velocity v = 0.3 ms^{-1}, no control (NC), time-invariant control (Ti) and time-varying system control (Tv).

Following Fig. 5 it is clear that a full state feedback controller cannot be used given the lack of accuracy of the state estimation. Also, the controllability matrix of the system (16) is not full rank which indicates that not all of the states might be controllable as well. The best matches of the modal coordinates towards the numerical model are achieved for the estimated states $[q_1\ q_2\ \dot{q}_1]$ as defined in section 5.1.

The influence on the deflection reduction, using a reduced order controller, is considered for a mass m = 0.261 kg moving at a speed v = 0.55 ms^{-1}. Three runs were taken per method. The value for the maximum displacement was averaged over the three runs. Fig. 7 displays the experimental relative maximum deflection at sensor x_{s2} for the time-invariant control method (left) in comparison with the time-varying control method (right) using different combinations of controlled states. It can be observed that a time-invariant controller only using one state q_1 provides a reduction of the maximum deflection of about 15%. The deflection reduction decreases even more when using more states leading to even a slight increase when using all states, which might be due to inaccuracies of the mode estimation. In contrast, the time-varying control method is applicable for the states $[q_1\ q_2\ \dot{q}_1]$ as well, with a reduction of about 15%. Using only the first state results in the best deflection reduction at x_{s2} of about 20%. Although using further states results in a complete solution of the problem, due to the lack of accuracy of the estimated states, the beam deflection is not improved. A different value of **Q** with an even higher weight towards the first modal displacement and modal velocity might lead to a higher reduction of the deflection if more of the states are used.

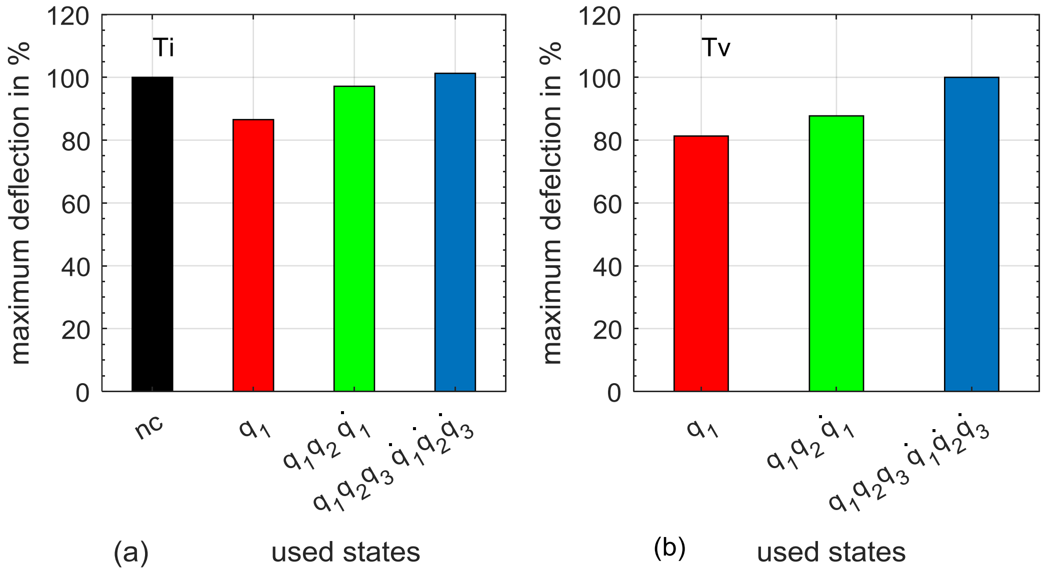

Fig. 7 Relative maximum deflection measured at sensor location x_{s2} normalized to the uncontrolled structure (nc) of the time-invariant control (Ti) (a) and the time-varying control (Tv) (b) from using one state to using all states.

Fig. 8 shows the time histories of the varying gains k_1, k_2 and k_4 corresponding to the states $[q_1\ q_2\ \dot{q}_1]$. The tests were run for the masses m = 0.261 kg, m = 0.371 kg and m = 0.509 kg traveling at the speed v = 0.3 ms^{-1}. Towards the time of t = 0.8 s the traveling mass reaches the moving coordinate $vt = 0.24$ m where the beam has the highest deflection (see Fig. 6). Consequently, the gains k_1 and k_2 increase up to this time. With that, a higher actuation is achieved when the action of the mass is high. Subsequently the gains decrease. When the mass passes by x_a = 0.5 m the gains k_1 and k_2 reach their minimum. The least amount of force is required to counteract the influence of the moving mass. In this way, an effective and stable control is achieved.

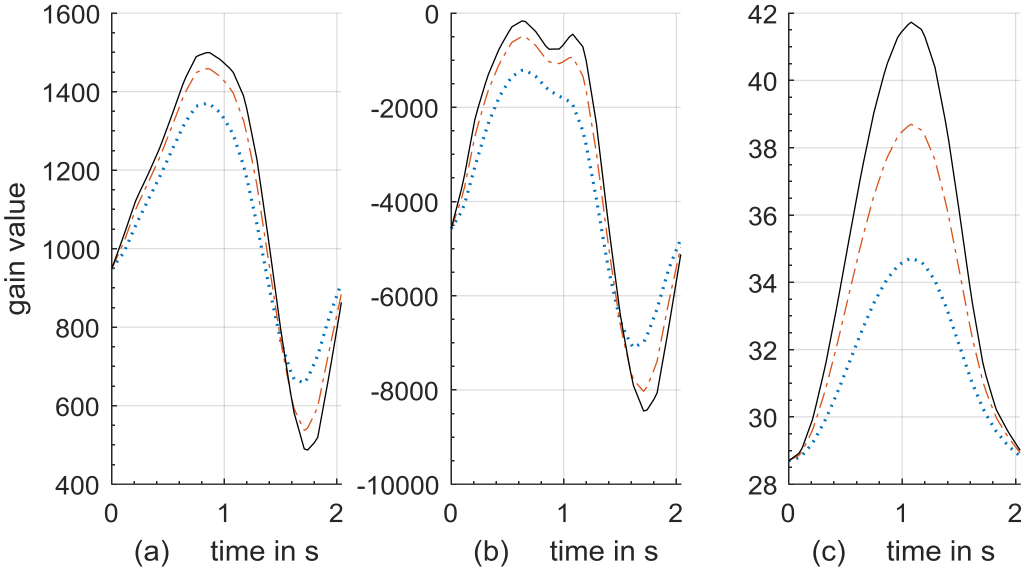

Fig. 8 Development of the time-varying gains $k_1(t)$ (a), $k_2(t)$ (b) and $k_4(t)$ (c) for the four different masses m = 0.261 kg (blue dotted), m = 0.371 kg (red dashed) to m = 0.509 kg (black continuous) at velocity v = 0.3 ms^{-1}.

In the following investigations the states $[q_1\ q_2\ \dot{q}_1]$ are used for control. This represents a fair compromise between completeness of the solution and reduction of the structural deflection.

To assess the stability of the time-varying system ($\mathbf{A}(t)$-$\mathbf{B}(t)\mathbf{k}(t)$), where the proposed reduced order controller is applied, its eigenvalues are calculated at certain time steps. Fig. 9 illustrates the course of the first four resulting complex conjugate pole pairs. During the time the mass m=0.509 kg travels with v =0.55 ms^{-1} over the beam the eigenfrequencies of the modes change, the poles circle in the negative left half plane around the time-invariant poles (black crossed). The system stays stable for this parameter.

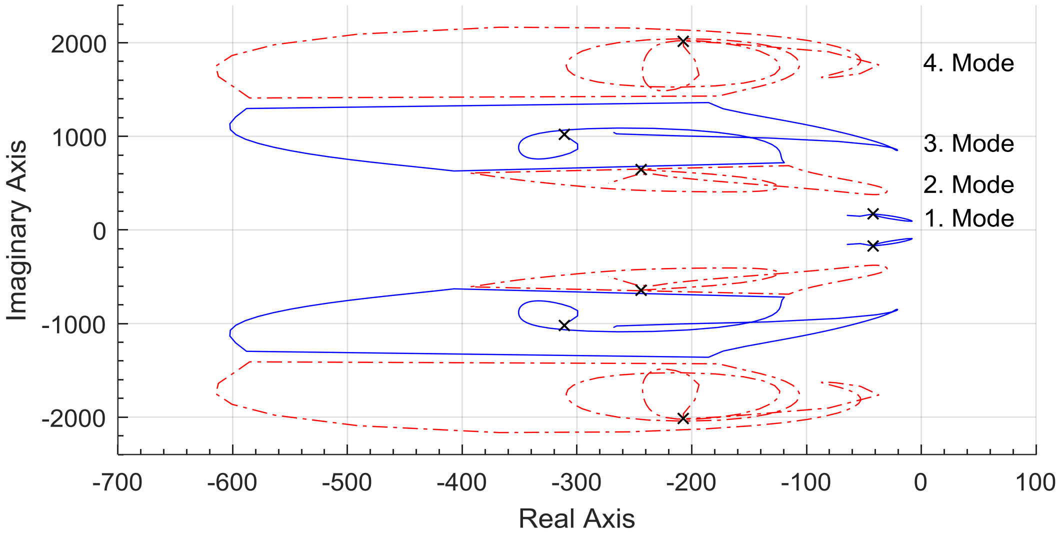

Fig. 9 Time history of the poles of the time-varying controlled system, first and third mode (blue continuous), second and fourth mode (red dashed), poles of the time-invariant system (black crossed), *m*=0.5 kg, *v*=0.55 m/s

Fig. 10(a) shows the poles of the simulated system with the reduced order controller and a traveling mass *m*= 0.509 kg. For the increased traveling speed of 5.6 m/s one pole pair moves into the real half plane causing instability. At this margin the full state controller (Fig. 10(b)) stays stable with all the poles in the negative half plane. Higher velocities and weights cause also with the full-state control instability. Likewise increasing the mass over *m*=6.5 kg with a low speed of 0.55 m/s some poles will move into the real half plane. In this way the theoretical stability margins of the system can be simulated. The additional actuator pole located at -10000 on the real axes is not shown in the figures.

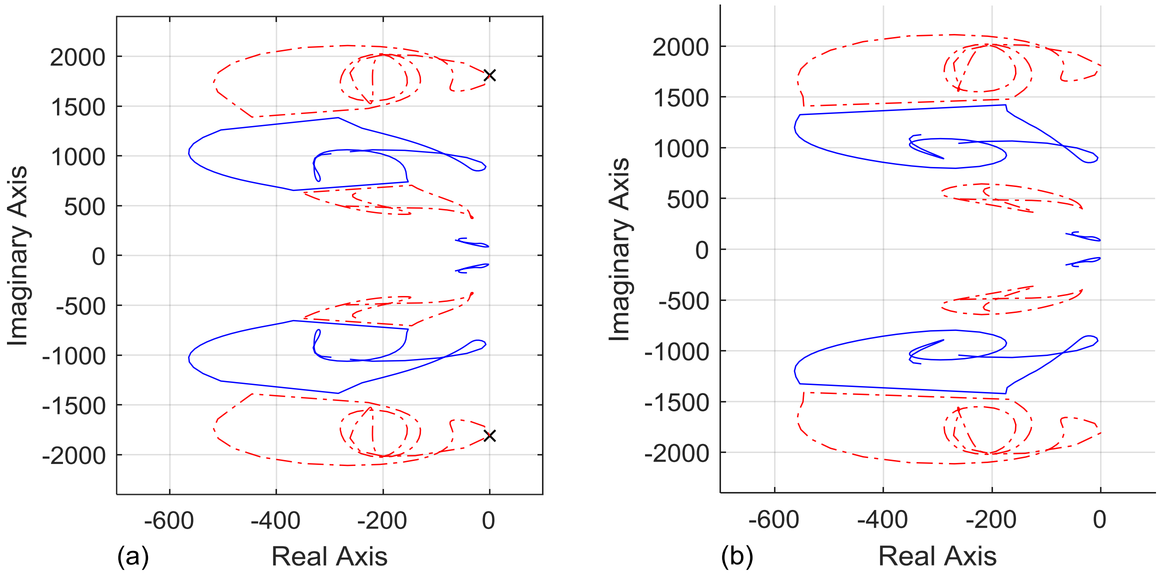

Fig. 10 Comparison of the first four poles of the time-varying system with the reduced order controller (left) and with the full state controller (rigth) instable poles (black asteriks) , m = 0.5 kg, v = 5.6 m/s

In order to assess the reduction of the maximum deflection at sensor location x_{s2} depending on the used control method three masses were tested at two speeds v = 0.3 ms^{-1} and v = 0.55 ms^{-1}. Five runs for each mass were averaged for the calculation of maximum deflections. The relative maximum deflections in Table 1 show a small reduction for the time-invariant control of around 3% for all the masses. The time-varying control shows a better performance for all the tests with a deflection reduction from 12% for m=0.261 kg to 17% for m= 0.509 kg, with a higher reduction for higher masses.

Table 1 Relative maximum deflection at x_{s2} for different masses traveling at v =0.3 ms^{-1}in percent.

mass m in kg	**no control**	**time-invariant**	**time-varying**
0.261	100	96.9	88
0.371	100	97.7	85.7
0.509	100	96.6	83.2

Fig. 11 illustrates the results obtained for mass m = 0.509 kg with a traveling speed of v = 0.3 ms^{-1}. It also shows a good agreement between the numerically calculated results and the experimentally measured deflection $w(x_{s2})$. There is a small mismatch after the mass leaves the beam due to the not modelled back electro-magnetic force (Back EMF) of the electromagnetic shaker [31].

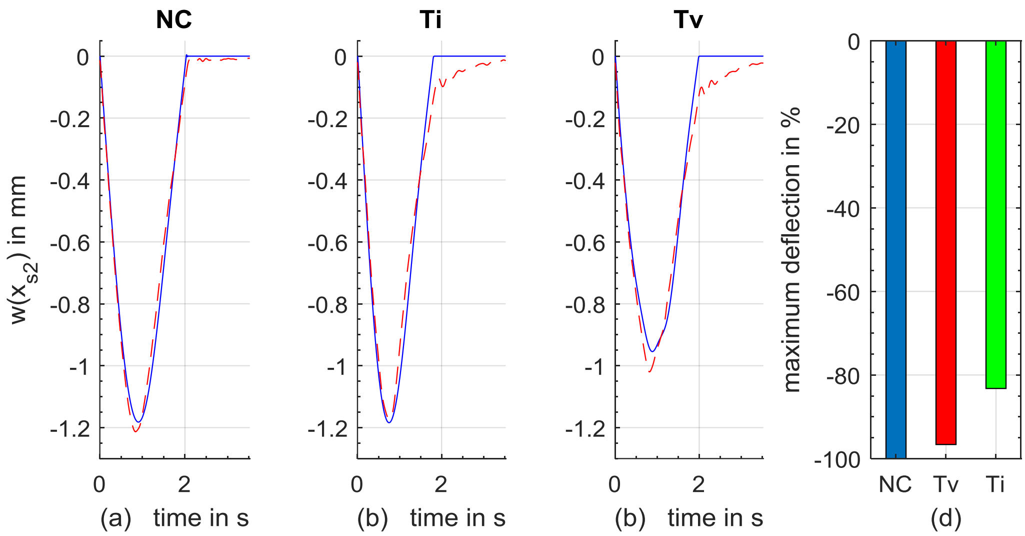

Fig. 11. Mass m = 0.509 kg moving with v = 0.3 ms^{-1}, comparison of the displacement $w(x_{s2})$ for the numerically calculated data (blue-continous) and the experimentally measured data (red dashed), for the case without control (a), with the time-invariant control (b),with the time-varying control (c) and the values of the relative maximum deflection in percent (d).

Fig. 12 illustrates the time history of the experimental control inputs $u(t)$ belonging to this example. It is noticed that the time-variant control has a high actuation especially in the first half of the traveling time whereas the time-invariant control is much less active in the first half.

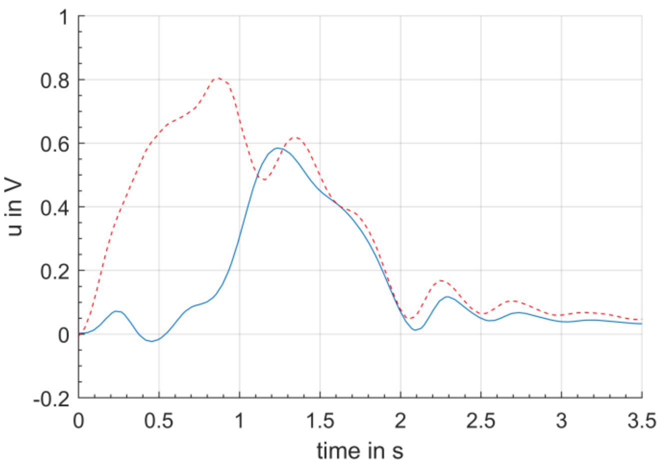

Fig. 12 Time-history of the experimentally measured control input, time-invariant (blue-continuous) and time variant (red- dashed)

Table 2 shows the relative maximum deflections for three masses moving with a higher speed v = 0.55 ms^{-1}. The invariant control reduces the maximum deflection only by 1% for mass m = 0.261 kg and by 8% for mass m = 0.509 kg. In contrast, the time-varying control achieves a reduction of approximately 18% for mass m = 0.509 kg. Again, it can be observed that the control is more effective for higher masses, as a higher deflection results in higher actuation. The results are similar for the two investigated velocities.

Table 2 Relative maximum deflection measured at x_{s2} for different masses traveling at v = 0.55 ms^{-1} in percent.

mass in kg	no control	time-invariant	time-varying
0.261	100	99.2	87.2
0.371	100	97.1	83
0.509	100	92	82.1

Fig. 13 shows one example of the beam deflection at sensor location x_{s2} when mass m = 0.261 kg moves with velocity v = 0.55 ms^{-1}. The measured deflections show a good match with the numerical model for all the tests with the only discrepancy observed after the mass leaves the structure due to back EMF of the electro-dynamic shaker. The time-varying controller reaches a reduction of 13%. A stable control with reduction of the beam deflection is achieved for different masses traveling at different speeds.

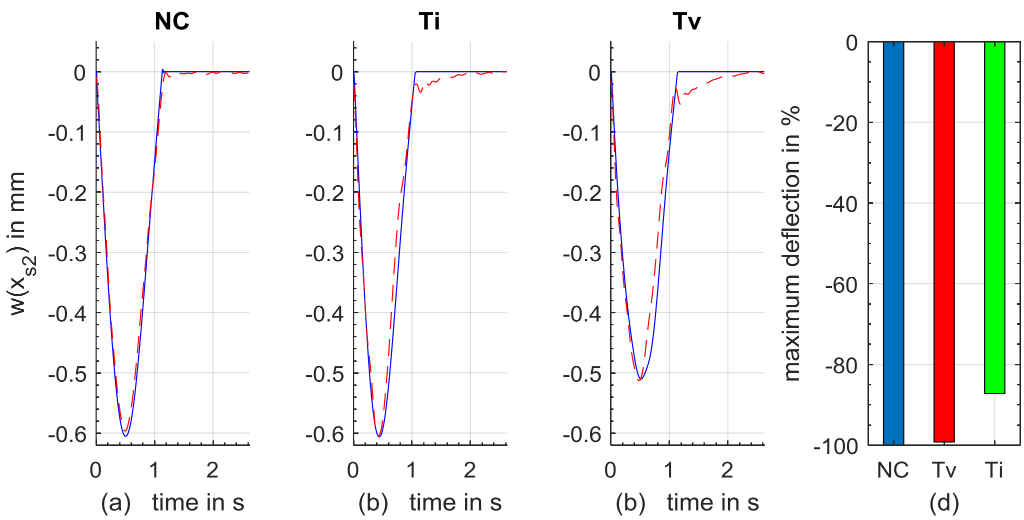

Fig. 13. Mass m = 0.261 kg moving with v = 0.55 ms^{-1}, comparison of the displacement $w(x_{s2})$ for the numerically calculated data (blue-continous) and the experimentally measured data (red dashed), for the

case without control (a), with the time-invariant control (b),with the time-varying control (c) and the values of the relative maximum deflection measured at x_{s2} in percent (d).

5.3 Experimental results for variable control gains

Following the experimental tests, it becomes clear that the performance of the controller depends on the weight of the moving mass. This means that a control gain that was designed to achieve a good reduction for a heavy mass may provide a too high control effort for a smaller mass whereas a controller gain designed for a small mass may not be enough to provide a good reduction of the deflection for a heavier mass. Therefore in terms of absolute deflection, the control effort required to achieve a prescribed absolute maximum deflection needs to change for the case when a small mass travels along the beam as compared to the case a heavier mass acts upon the beam.

In this respect a gain scheduling of the control gain either as $\mathbf{k}(m)$ a function of mass or as $\mathbf{k}(m,v)$ a function depending on both mass m and speed v is tested. The masses used are m_1=0.261 kg, m_2=0.322 kg, m_3=0.371 kg and m_4=0.509 kg.

Fig. 14 shows the effect of using the specific scheduled time-varying gains $\mathbf{k}(m_1)$, $\mathbf{k}(m_2)$, $\mathbf{k}(m_3)$ and $\mathbf{k}(m_4)$, calculated taking into account every mass, compared with the time-varying gain $\mathbf{k}(m_1)$ determined for mass m_1 and subsequently used for all masses. In this way the control switches to the specific control gain, therefore a heavier mass will have a higher control gain that will confine the deflection of the beam within a prescribed limit (in this case about 1 mm). Fig. 14 shows a gradual reduction of the deflection as the gain increases with the weight of the mass.

With this approach where the gains are scheduled taking into account the value of the mass, the relative maximum deflection is 10% lower compared to the unscheduled control using the gain of the first mass $\mathbf{k}(m_1)$ all over, see Fig. 15. The performance of this method can be improved if the gains are determined taking into account the moving mass into the system equation as an augmented system, introduced in [4]. The gains can be scheduled based on deflection values in the first phase. On a real bridge-like structure, image processing or a scale can identify the actual load case of m and select the optimal gain for control.

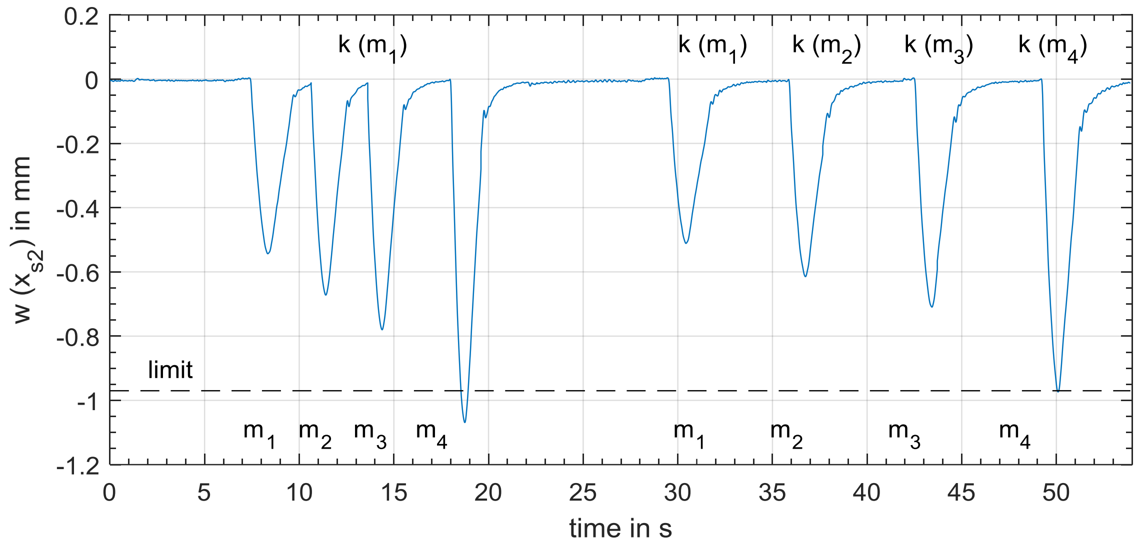

Fig. 14. Effect of using time-varying gain $\mathbf{k}(m_1)$ (left) and scheduled for each mass specifically (right) $\mathbf{k}(m_1)$ – $\mathbf{k}(m_4)$.

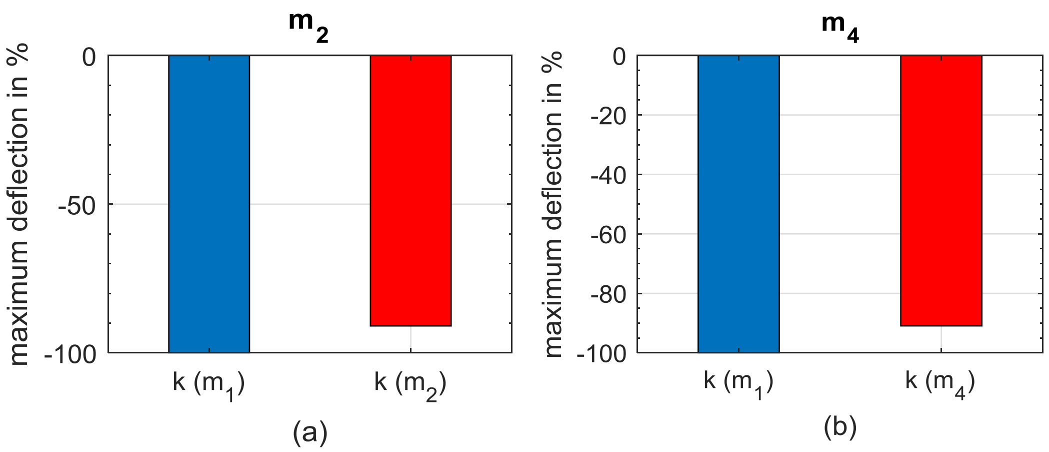

Fig. 15. Relative maximum deflection for mass m_2 (a) and mass m_4 (b) using gain $\mathbf{k}(m_1)$ (blue) in comparison to using the specific gains $\mathbf{k}(m_2)$ or $\mathbf{k}(m_1)$ (red).

Another important factor of the proposed control strategy is the ability to adapt to different velocities of the mass. The time-varying gain vector $\mathbf{k}(t,m)$ is calculated beforehand for a predetermined velocity at equal time steps and stored on the controller. By measuring the actual velocity in real time using two induction sensors before the mass enters the structure, the leaving time t_f can be determined exactly. With the given t_f the control action is stretched or compressed towards the given traveling time of the mass. The gain is then interpolated between the precalculated gain values for the actual position of the mass.

In Fig. 16 it can be seen how the control needs to adapt to different speeds ranging from $v = 0.22\ \mathrm{ms}^{-1}$to $v = 0.95\ \mathrm{ms}^{-1}$. The gain $k_1(m_4)$ calculated in real time coincides well with the numerically calculated gain.

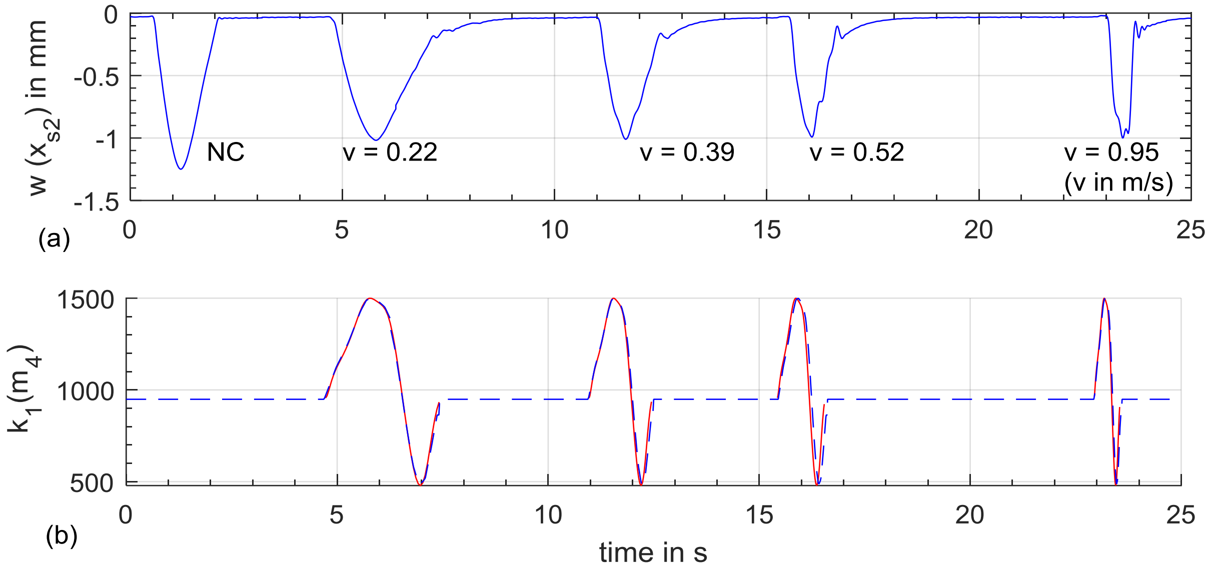

Fig. 16. Deflection $w(x_{s2})$, no control action (NC) and with different speeds v (a); time-varying gain $k_1(m_4)$ (b) calculated in real-time (blue-dashed) and numerically (red- continuous) .

6. Conclusion and future work

The present study extends numerical investigations into the problem of control of beam structures subjected to a set of moving masses, and is concerned with the experimental implementation of the control solution on a small-scale rig.

It presents and analyses the synthesis and implementation of an active controller on a small-scale test structure. The structure is modelled as a simply supported beam, using displacement laser sensors and one electromagnetic actuator located close to one of the supports. The importance of this study consists on going beyond the theoretical solution to finding and validating solutions based on experimental data. In this way the proposed solutions are one step closer to the relevant practical problem.

Due to the fast sampling rate of the data acquisition and control, a reduced order controller using estimated modal displacements and velocities proves to be the best solution. The dynamics of the actuator was simplified, and a first order model was used. Although the model proved correct while contact is maintained, a small inaccuracy is observed when the mass leaves the beam.

As expected, due to the time-varying nature of the control system, it is shown both experimentally and numerically that a control method based on a terminal-time optimal control solution provides better performance than a time invariant optimal controller.

The possibility of using different moving masses travelling at different speeds also pointed toward a control solution that adapts the control effort, taking into account the type of load. Therefore, a simple gain-scheduling solution that makes a better use of the control effort is presented and proves to be the basis of further work and developments of the method.

Acknowledgements

The author acknowledges the financial support of the Faculty of Engineering and Technology at Liverpool John Moores University.

References

[1] Stancioiu, D., James, S., Ouyang, H., and Mottershead, J. E., 2009, "Vibration of a Continuous Beam Excited by a Moving Mass and Experimental Validation," *Journal of Physics: Conference Series*.

[2] Ouyang, H., 2011, "Moving-Load Dynamic Problems: A Tutorial (with a Brief Overview)," Mechanical Systems and Signal Processing, **25**(6), pp. 2039–2060.

[3] Korkmaz, S., 2011, "A Review of Active Structural Control: Challenges for Engineering Informatics," Computers and Structures, **89**(23–24), pp. 2113–2132.

[4] Marcheggiani, L., and Lenci, S., 2010, "On a Model for the Pedestrians-Induced Lateral Vibrations of Footbridges," Meccanica, **45**(4), pp. 531–551.

[5] Yang, J., Ouyang, H., Stancioiu, D., Cao, S., and He, X., 2018, "Dynamic Responses of a Four-Span Continuous Plate Structure Subjected to Moving Cars With Time-Varying Speeds," J. Vib. Acoust. Trans. ASME, **140**(6), pp. 1–15.

[6] Visweswara Rao, G., 2000, "Linear Dynamics of an Elastic Beam under Moving Loads," J. Vib. Acoust. Trans. ASME, **122**(3), pp. 281–289.

[7] Frýba, L., 1999, *Vibration of Solids and Structures under Moving Loads*, Thomas Telford Publishing, Prague.

[8] Younesian, D., Kargarnovin, M. H., and Esmailzadeh, E., 2008, "Optimal Passive Vibration Control of Timoshenko Beams with Arbitrary Boundary Conditions Traversed by Moving Loads," Proceedings of the Institution of Mechanical Engineers, Part K: Journal of Multi-body Dynamics, **222**(2), pp. 179–188.

[9] Xiaomin Shi, and Cai, C. S., 2008, “Suppression of Vehicle-Induced Bridge Vibration Using Tuned Mass Damper,” Journal of Vibration and Control, **14**(7), pp. 1037–1054.

[10] Pierson, H., Brevick, J., and Hubbard, K., 2013, “The Effect of Discrete Viscous Damping on the Transverse Vibration of Beams,” Journal of Sound and Vibration, **332**(18), pp. 4045–4053.

[11] Debnath, N., Deb, S., and Dutta, A., 2016, “Multi-Modal Vibration Control of Truss Bridges with Tuned Mass Dampers under General Loading,” Journal of Vibration and Control, **22**(20), pp. 4121–4140.

[12] Adam, C., Di Lorenzo, S., Failla, G., and Pirrotta, A., 2017, “On the Moving Load Problem in Beam Structures Equipped with Tuned Mass Dampers,” Meccanica, **52**(13), pp. 3101–3115.

[13] Brecher, C., Fey, M., Brockmann, B., and Chavan, P., 2018, “Multivariable Control of Active Vibration Compensation Modules of a Portal Milling Machine,” Journal of Vibration and Control, **24**(1), pp. 3–17.

[14] Balas, M. J., 1978, “Active Control of Flexible Systems,” Journal of Optimization Theory and Applications, **25**(3), pp. 415–436.

[15] Inman, D. J., 2006, *Vibration with Control*, John Wiley & Sons, Ltd, Chichester, UK.

[16] Preumont, A., 2011, *Vibration Control of Active Structures*, Springer Netherlands, Dordrecht.

[17] Stancioiu, D., and Ouyang, H., 2016, “Optimal Vibration Control of Beams Subjected to a Mass Moving at Constant Speed,” Journal of Vibration and Control, **22**(14), pp. 3202–3217.

[18] Nikkhoo, A., Rofooei, F. R., and Shadnam, M. R., 2007, “Dynamic Behavior and Modal Control of Beams under Moving Mass,” Journal of Sound and Vibration, **306**, pp. 712–724.

[19] Nikkhoo, A., 2014, “Investigating the Behavior of Smart Thin Beams with Piezoelectric Actuators under Dynamic Loads,” Mechanical Systems and Signal Processing, **45**(2), pp. 513–530.

[20] Sung, Y. G., 2002, “Modelling and Control with Piezoactuators for a Simply Supported Beam under a Moving Mass,” Journal of Sound and Vibration, **250**(4), pp. 617–626.

[21] Deng, F., Rémond, D., and Gaudiller, L., 2011, “Self-Adaptive Modal Control for Time-Varying Structures,” Journal of Sound and Vibration, **330**(14), pp. 3301–3315.

[22] Naidu, D. S., 2003, *Optimal Control Systems*, CRC Press, Boca Raton.

[23] Pi, Y., and Ouyang, H., 2016, “Vibration Control of Beams Subjected to a Moving Mass Using a Successively Combined Control Method,” Applied Mathematical Modelling, **40**(5–6), pp. 4002–4015.

[24] Liu, X., Wang, Y., and Ren, X., 2020, “Optimal Vibration Control of Moving-Mass Beam Systems with Uncertainty,” Journal of Low Frequency Noise, Vibration and Active Control, **39**(3), pp. 803–817.

[25] Frischgesell, T., Popp, K., Reckmann, H., and Schütte, O., 1998, “Regelung Eines Elastischen Fahrwegs Unter Verwendung Eines Variablen Beobachters (Control of an Elastic Guideway by Use of a Variable Observer),” Technische Mechanik, **18**(1), pp. 45–55.

[26] Reckmann, H., and Popp, K., 2000, “Deflection and Vibration Control of an Elastic Guideway Under a Moving Mass,” IFAC Proceedings Volumes, **33**(26), pp. 947–952.

[27] Pisarski, D., 2018, "Optimal Control of Structures Subjected to Traveling Load," Journal of Vibration and Control, **24**(7), pp. 1283–1299.

[28] Pisarski, D., and Myśliński, A., 2018, "Online Adaptive Semi-Active Vibration Damping of Slender Structures Subject to Moving Loads," MATEC Web of Conferences, **148**, pp. 05006-.

[29] Sievert, L., Stancioiu, D., Matthews, C., Rothwell, G., and Jenkinson, I., 2019, "Numerical and Experimental Investigation of Time-Varying Vibration Control for Beam Subjected to Moving Masses," *International Conference on Structural Engineering Dynamics, ICEDyn*, Viana do Castelo, Portugal.

[30] Stancioiu, D., Ouyang, H., Mottershead, J. E., and James, S., 2011, "Experimental Investigations of a Multi-Span Flexible Structure Subjected to Moving Masses," Journal of Sound and Vibration, **330**(9), pp. 2004–2016.

[31] Waters, T. P., 2019, "A Chirp Excitation for Focussing Flexural Waves," Journal of Sound and Vibration, **439**, pp. 113–128.

List of Figures

Fig. 1 Model of the beam structure subjected to a moving mass, with an inactive actuator (a) and an active actuator (b). 5

Fig. 2 Experimental set-up, aluminium polymer beam subjected to a moving mass. 11

Fig. 3 Experimental validation between the displacements of masses traveling at different speeds obtained by the numerical model (blue continuous) and the experimental measurements (red dashed). 12

Fig. 4 Validation of the beam mass system with an active electromagnetic shaker, numerical model (blue continuous), and the experimental measurements (red dashed). 13

Fig. 5 Comparison modal coordinates and modal velocieties, numerical model (black dashed) and the measured signal (blue continuous). 13

Fig. 6 Numerical deflection of the moving coordinate vt of the mass m = 0.5 kg traveling with velocity v = 0.3 $ms-1$, no control (NC), time-invariant control (Ti) and time-varying system control (Tv). 15

Fig. 7 Relative maximum deflection measured at sensor location $xs2$ normalized to the uncontrolled structure (nc) of the time-invariant control (Ti) (a) and the time-varying control (Tv) (b) from using one state to using all states. 16

Fig. 8 Development of the time-varying gains $k_1(t)$ (a), $k_2(t)$ (b) and $k_4(t)$ (c) for the four different masses m = 0.261 kg (blue dotted), m = 0.371 kg (red dashed) to m = 0.509 kg (black continuous) at velocity v = 0.3 ms^{-1}. 17

Fig. 9 Time history of the poles of the time-varying controlled system, first and third mode (blue continuous), second and fourth mode (red dashed), poles of the time-invariant system (black crossed), m=0.5 kg, v=0.55 m/s 18

Fig. 10 Comparison of the first four poles of the time-varying system with the reduced order controller (left) and with the full state controller (rigth) instable poles (black asteriks) , m = 0.5 kg, v = 5.6 m/s 19

Fig. 11. Mass m = 0.509 kg moving with v = 0.3 ms^{-1}, comparison of the displacement $w(x_{s2})$ for the numerically calculated data (blue-continous) and the experimentally measured data (red dashed), for the case without control (a), with the time-invariant control (b),with the time-varying control (c) and the values of the relative maximum deflection in percent (d). 20

Fig. 12 Time-history of the experimentally measured control input, time-invariant (blue-continuous) and time variant (red- dashed) 20

Fig. 13. Mass m = 0.261 kg moving with v = 0.55 ms^{-1}, comparison of the displacement $w(x_{s2})$ for the numerically calculated data (blue-continous) and the experimentally measured data (red dashed), for the case without control (a), with the time-invariant control (b),with the time-varying control (c) and the values of the relative maximum deflection measured at $xs2$ in percent (d). 21

Fig. 14. Effect of using time-varying gain $\mathbf{k}(m_1)$ (left) and scheduled for each mass specifically (right) $\mathbf{k}(m_1)$ – $\mathbf{k}(m_4)$. 23

Fig. 15. Relative maximum deflection for mass m_2 (a) and mass m_4 (b) using gain $\mathbf{k}(m_1)$ (blue) in comparison to using the specific gains $\mathbf{k}(m_2)$ or $\mathbf{k}(m_1)$ (red). 23

Fig. 16. Deflection $w(x_{s2})$, no control action (NC) and with different speeds v (a); time-varying gain $k1(m4)$ (b) calculated in real-time (blue-dashed) and numerically (red- continuous) . 24

List of Tables

Table 1 Relative maximum deflection at $xs2$ for different masses traveling at v =0.3 $ms-1$in percent. 19

Table 2 Relative maximum deflection measured at $xs2$ for different masses traveling at v = 0.55 ms^{-1} in percent. 21